Editors' Suggestion

Pressure and strain effects on the *ab initio GW* electronic structure of $La_3Ni_2O_7$

Jean-Baptiste de Vaulx,[1] Quintin N. Meier,[1] Pierre Toulemonde,[1] Andrés Cano,[1] and Valerio Olevano[1,2]
[1]*Université Grenoble Alpes, CNRS, Institut Néel, 25 Rue des Martyrs, 38042 Grenoble, France*
[2]*ETSF, European Theoretical Spectroscopy Facility, 38000 Grenoble, France*

(Received 30 April 2025; revised 11 July 2025; accepted 29 July 2025; published 25 August 2025)

The recent discovery of superconductivity in $La_3Ni_2O_7$ at a critical temperature above 80 K points to a nonconventional pairing mechanism in nickelates as in cuprates, possibly due to electronic correlations. We have calculated from first principles the electronic structure of $La_3Ni_2O_7$ under the effect of pressure and epitaxial strain including correlations by the *GW* approximation to the many-body self-energy. We find that the Fermi surface is composed of a characteristic cuprate-shape sheet β plus a nickelate-specific cylinder α, both from Ni e_g orbitals, with a nonnegligible drop in the quasiparticle weight and an effective 1D character. This topology results from a delicate balance between the Ni-$3d_{z^2}$ hole pocket γ, which is suppressed by correlations, and an emerging La-$5d_{x^2-y^2}$ electron pocket induced by both correlation and pressure/strain effects and whose role at low energy has been neglected so far. Unlike cuprates, the electronic structure of $La_3Ni_2O_7$ is already correctly described from *ab initio* and in agreement with the experiment without the need to introduce adjustable parameters.

DOI: 10.1103/q5ym-hf5k

I. INTRODUCTION

The recent discovery of superconductivity (SC) in Ruddlesden-Popper (RP) nickelates [1–3] has introduced a new direction in the field of high-temperature superconductivity. Notably, superconductivity has been observed in bulk samples of the bilayer $La_3Ni_2O_7$ under high pressure [1], with the superconducting phase forming a right-triangular region spanning 14 to 80 GPa, and reaching a maximum onset critical temperature T_c of approximately 80 K at 18 GPa [4]. More recently, superconductivity has also been reported at $T_c \sim 40$ K in $La_3Ni_2O_7$ thin films under epitaxial compressive strain at ambient pressure [5,6]. While the superconducting mechanism is still debated in infinite-layer $LnNiO_2$ nickelates [7–11], where critical temperatures do not overstep 30 K [12,13], the high critical temperature observed in $La_3Ni_2O_7$ is difficult to reconcile with a BCS electron-phonon pairing mechanism [14,15], thus pointing to unconventional superconductivity like in cuprates. Indeed, cuprates and nickelates share many analogies: they are both organized in a layered crystal structure with CuO_2 or NiO_2 planes; and present the same "cuprate-shape" Fermi surface sheet of main $3d_{x^2-y^2}$ character, although nickelates bilayer and trilayer show a strong Ni-$3d_{z^2}$ hybridization in the antinodal direction. However, there are also important differences: the constant presence of an antiferromagnetic insulating parent phase in cuprates has no analogous in nickelates. For what concerns the electronic structure, the fact that in nickelates the Ni-$3d_{z^2}$ states are closer to the Fermi level than in cuprates, gives rise to at least another Fermi sheet and possibly to a multiband character superconductivity. Therefore, although both unconventional, the pairing mechanism could be possibly different in cuprates and nickelates.

Interestingly, unconventional superconductivity was anticipated on a theoretical basis in $La_3Ni_2O_7$ by invoking finite-energy spin fluctuations as pairing glue [16]. Then many other different model theoretical pictures [17–48] have been proposed to explain the superconductivity in the bilayer. The symmetry of the superconducting state remains unclear as subsequent studies have indicated the possibility of not only $s_\pm$-wave but also d-wave pairing states including d_{xy}-wave, depending on specific details of the electronic structure [24,31,34,49–52]. Also the respective role of the two Ni-$3d$ e_g orbitals in the superconducting mechanism is still under discussion [53]. With respect to spin fluctuations, the gap between the two upper and lower Ni-$3d_{z^2}$ bands, originating from the interlayer hopping, seems to be relevant [24]. The presence or absence of the so-called γ hole pocket in the Fermi surface, that should arise from the lower Ni-$3d_{z^2}$ band, is still unclear both in theoretical calculations [45,54,55] and in experimental angle-resolved photoemission spectroscopy (ARPES) measurements [56,57]. Regardless of its presence or not at the Fermi level, this band is believed to be important in the pairing mechanism [58]. All the previous points require a correct description of the electronic structure including electronic correlations.

In this work we study from *ab initio* the electronic structure of $La_3Ni_2O_7$ including correlations at the level of the *GW* approximation to the self-energy [59–62]. In contrast to the Kohn-Sham eigenvalues used in density-functional theory (DFT), which are the energies of a fictitious noninteracting system, *GW* quasiparticle energies have a direct physical interpretation as the excitation energies measured in ARPES. The *GW* approximation takes into account electronic exchange and correlations without introducing any adjustable parameter, neither in the DFT functional (e.g., an α hybrid mixing parameter) nor in the Hamiltonian (e.g., a Hubbard U interaction term). The weight of correlation effects and their importance in this system is revealed by a comparison between the *GW* electronic structure and the DFT band plot. However, in this work we applied the one-iteration G_0W_0 approach which can keep some reminiscence of the DFT starting point.

We also investigate the electronic structure evolution of bulk $La_3Ni_2O_7$ with respect to pressure, as well as in presence of in-plane constraints that simulate a thin film grown on a substrate. Our purpose is to highlight aspects which might be relevant to explain superconductivity that in this system is induced by pressure without doping. The focus is at the Fermi level but also at higher energy features which are less affected by the estimated 0.1 eV best *GW* absolute accuracy, and which might be relevant in the competition between different pairing symmetries according to some proposed superconducting mechanisms [24]. Our work describes some of the electronic structure features expected to be relevant by theoretical models so far proposed [17–48] and provides also indications for future works.

The paper is organized as follows: after introducing our methods in Sec. II, we will first compare our *GW* calculations with previous *ab initio* works done at 29.5 GPa with the crystal structure used by almost all DFT as well as two *GW* calculations [15,45] (Sec. III A). We will then show the evolution with pressure of the electronic structure for the bulk crystal in Sec. III B, and finally introduce in Sec. III C our *GW* results for the structure with epitaxial strain of 1.8%. Our results will be compared with the available experimental data from photoemission (ARPES) experiments.

II. CALCULATION DETAILS

A. Numerical methods

Our methodology relies as a first step on density-functional theory (DFT) calculations in the PBE approximation [63], using the plane waves code ABINIT [64]. We use norm-conserving pseudopotentials from the PseudoDojo table library [65]. The La pseudopotential takes $4f$ electrons in conduction and does not freeze them in the core. We have used a $16 \times 16 \times 16$ standard sampling of the Brillouin zone (BZ) and a plane waves (PW) cutoff of 65 Ha for the DFT-PBE starting calculation, as well as a Gaussian smearing of 0.01 Hartree. In the subsequent *GW* calculations, the BZ sampling has been reduced to $6 \times 6 \times 6$, whereas the PW cutoffs have been reduced to 40 Ha for the representation of the wave functions and for the exchange self-energy, and further down to 15 Ha for the correlation self-energy and the screening. We included 187 bands for the calculation of the screening and 225 for the self-energy (see Sec. VII in the Supplemental Material [66] for convergence studies). We have carried just only one *GW* iteration (i.e., G_0W_0) on top of PBE, using a Godby-Needs plasmon-pole model [67] and a shift of 0.1 eV to avoid poles/divergences. The final *GW* band plots, total and projected density of states (DOS and PDOS), as well as Fermi surfaces, were interpolated from the $6 \times 6 \times 6$ to a denser k-mesh by the WANNIER90 code using a set of 67 projected Wannier functions (PWFs) with the closest possible character to atomic orbitals, namely O-$2p$, Ni-$3d$, La-$5d$, and La-$4f$. The band orbital characters and PDOS identified by these PWFs are almost coincident with what one would obtain by projecting Bloch wave functions directly onto real (pseudo) atomic orbitals, as we have checked using the QUANTUM ESPRESSO code with equivalent parameters, which is not the case when selecting a set of maximally localized Wannier functions (MLWFs) (see Supplemental Material [66] Sec. V). In the bandplots showing projected orbital character, the width of the dots is proportional to the orbital contribution.

All calculations have been done with a Gaussian smearing temperature T_s of 0.01 Ha to ease self-consistency convergence and optical absorption onset stability (which in any case has little relevance on main plasmons, energy-loss and screening W). For the most critical case at $P = 29.5$ GPa we have checked that a calculation with T_s enforced at 10^{-4} Ha in both DFT and *GW* calculations provides the same physical picture, and in particular the same Fermi surface as in Fig. 1(b), with only minor adjustments of less than 10 meV on band positions, mostly due to the fact that the chemical potential μ at larger temperature is a less accurate estimate for the Fermi energy (see Supplemental Material [66] Sec. IV).

B. Crystal structure and Brillouin zone

To determine the crystal structure of $La_3Ni_2O_7$ at ambient pressure, and then in the superconducting range at 14, 29.5 and 40 GPa, we have performed DFT PBE structural relaxations which provided the $I4/mmm$ space group as the lowest energy structure at all considered pressures, except at 0 GPa where the *Amam* structure is more stable. Nevertheless, our *GW* calculations have all referred to the $I4/mmm$ structure even at ambient pressure to ease the comparison and better follow the evolution of the electronic structure with pressure, from the superconducting range down to 0 GPa. For all the cases we have used the relaxed lattice parameters and the internal atomic position out of our PBE relaxations, except for the case at 29.5 GPa which we treated separately.

Indeed, 29.5 GPa is the most studied case in the theoretical literature, so that we use it as a benchmark case to compare with previous calculations. Thus, for the sake of comparison, we decided to stick to the lattice parameters and atomic positions used in most of previous works [24,45]. Therefore, we consider a tetragonal $I4/mmm$ structure with $a = 3.715$ Å and $c = 19.734$ Å as Sakakibara *et al.* [24]. In fact, instead of the initial $Fmmm$ space-group symmetry proposed for $La_3Ni_2O_7$ at 29.5 GPa, our calculations predict the $I4/mmm$ space-group symmetry with lattice parameters that are in good agreement with the experimental ones [68]. Further, in Ref. [45], it was noticed that the electronic structure of $La_3Ni_2O_7$ at 29.5 GPa is extremely sensitive to internal atomic positions and that the experimental ones reported by Sun *et al.* from the x-ray diffraction [1] likely yield artifacts at the Fermi level. We provide a detailed analysis of this question in Supplemental Material [66] Sec. II.

To simulate epitaxial strain, we enforced the tetragonal a lattice parameter to the experimentally observed value of 3.77 Å [5] and let the system relax in the z direction, which provided $c = 20.293$ Å. This crystal structure corresponds to a bulk nonhydrostatic planar stressed system, or equivalently a system pulled along the c axis, that we will use to simulate an epitaxially strained thin film. All our crystal structures are detailed in Supplemental Material [66] Sec. I.

All our electronic structures are reported in the $I4/mmm$ body-centered tetragonal (BCT) Brillouin zone (BZ) which we report in Fig. 1(c) by black lines, while the blue line shows the path followed in our band plots with k-point labels

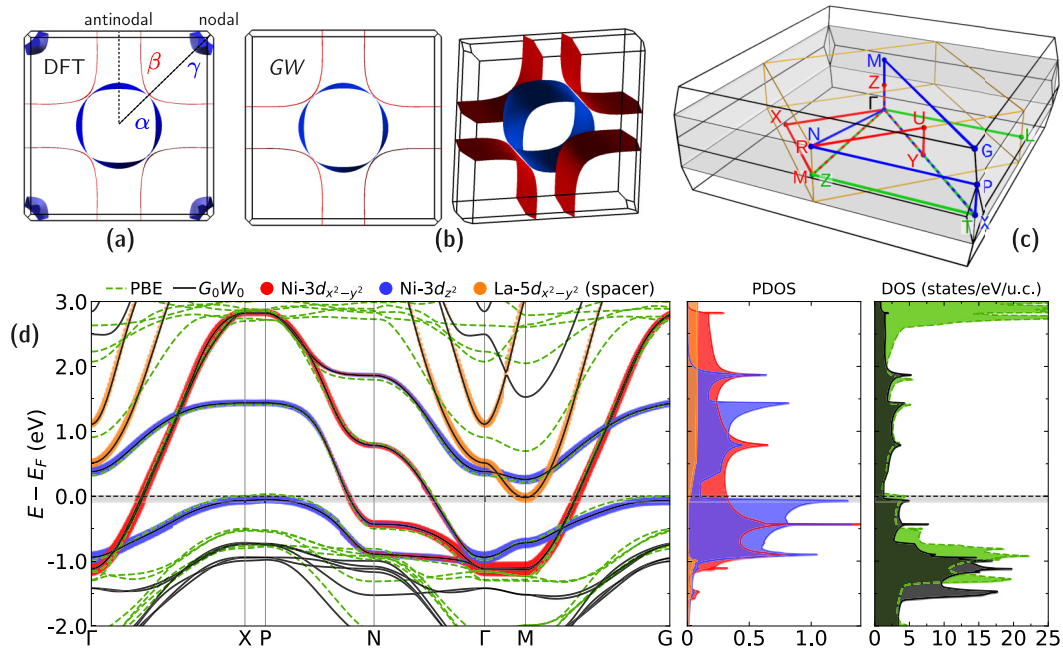

FIG. 1. Fermi surfaces of $La_3Ni_2O_7$ at 29.5 GPa within the body-centered tetragonal (BCT) Brillouin zone (BZ) calculated for the DFT-PBE (a) and the *GW* (b) approximation. The Fermi sheets α and β are shown in blue and red, respectively. The blue sheets at the BZ corners are the Ni-3d_{z^2} hole pockets, labeled γ. (c) Comparison between different BZs and k-paths: the primitive BCT (black lines) and k-path [69] (blue line) corresponding to the $I4/mmm$ structure used in this work; the simple tetragonal BZ (gray box) associated with the conventional cell; the simple orthorhombic BZ (orange lines) and k-path (red line) referred by the ARPES work Ref. [56] in which they referred to the tilted *Amam* structure requiring an $\sqrt{2} \times \sqrt{2} \times 2$ supercell with respect to our cell; and finally the k-path of Christiansson *et al.* [45] (green) in the simple orthorhombic BZ corresponding to the *Fmmm* structure. All orthorhombic BZs have been tetragonalized to ease the visualization. (d) PBE (dashed green) and G_0W_0 (black) band plots of $La_3Ni_2O_7$ at 29.5 GPa in the BCT Brillouin zone and along the k-path already indicated in panel (c). Relevant orbital character projections are plotted for G_0W_0, namely Ni-3$d_{x^2-y^2}$, Ni-3d_{z^2} and La-5$d_{x^2-y^2}$ (restricted to atoms of the spacer for the latter). The corresponding DOS and PDOS are shown on the right. The gray stripe shows the estimated uncertainty interval of 100 meV for the Fermi level, and the thin black dashed line the E_F value calculated by ABINIT, chosen as the origin of the energy axis (see Supplemental Material [66] Sec. IV).

using the convention of Hinuma *et al.* [69]. Notice that in this convention, the X and M k-points do not correspond to the canonical ones used in the 2D BZ of the square lattice widely used in the model literature: X is at the BZ corner in the nodal direction and M lies in the $k_z = 2\pi/c$ plane. We also indicate in gray the BZ corresponding to the conventional cell, namely simple tetragonal, which ease the comparison with 2D BZs. In the same Fig. 1(c), we report also the simple orthorhombic BZ and associated k-path to compare with the ARPES experiment [56] which referred to the tilted *Amam* structure needing a $\sqrt{2} \times \sqrt{2} \times 2$ supercell compared to ours; and finally the face-centered orthorhombic BZ (and associated k path) to compare with the calculation of Christiansson *et al.* [45] who referred to the $Fmmm$ crystal structure.

III. RESULTS

A. Electronic structure at 29.5 GPa

We start discussing the electronic structure of $La_3Ni_2O_7$ at the pressure of 29.5 GPa over which most of previous theoretical calculations have been performed. Our PBE and *GW* Fermi surfaces are shown in Figs. 1(a) and 1(b), while Fig. 1(d) shows the corresponding band structures. In the same figure, selected orbital character contributions are plotted on the *GW* band structure, as well as the projected densities of states (PDOS) and the total density of states (DOS).

We briefly mention that, like it was already found [7,8,70] in infinite-layer nickelates, e.g., $LaNiO_2$, *GW* correlations shift 2 eV up the flat bands with predominant La-4f character, moving them further away from the Fermi level and out of the low-energy region, and shift 1 eV down the O-2p manifold, leading to an increased ionic charge-transfer energy between Ni-3d and O-2p states. These aspects were previously detailed [70] and will not be again discussed here where we focus on the low-energy region.

1. Ni e_g Fermi surface sheets

The Fermi level is dominated by bands with Ni-3d e_g character. The DFT PBE Fermi surface consists of three sheets, labeled α, β, and γ in previous literature [18]. The α sheet is a large cylindrical sheet centered around Γ; β is the sheet with the characteristic shape of the cuprate Fermi surface; and γ is a small hole pocket located at the Brillouin zone (BZ) corners which is highly dispersive along k_z. The α and β sheets are primarily of $d_{x^2-y^2}$ character, though they show significant hybridization with d_{z^2} orbitals in the antinodal direction, as well as with O-2p states [see Fig. 2(b)]. In contrast, the γ

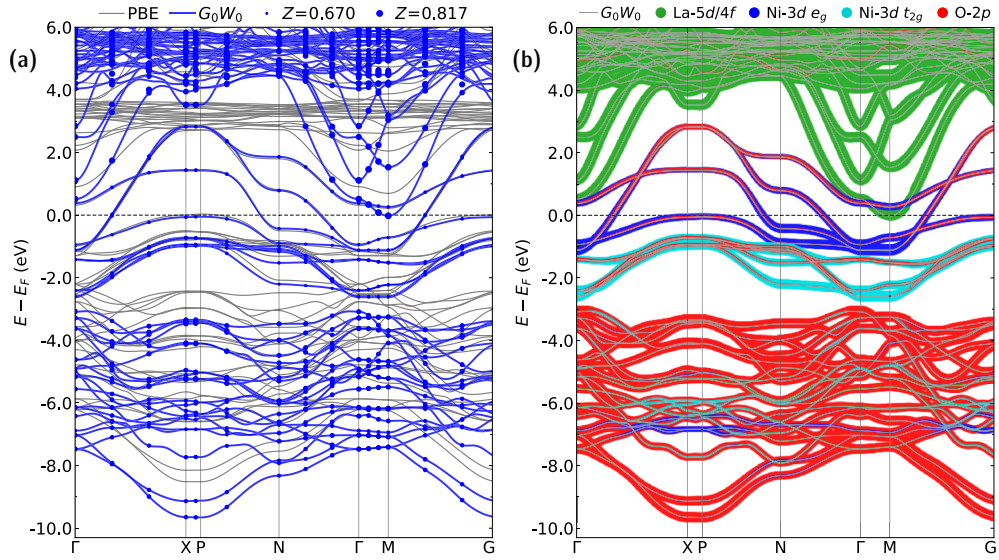

FIG. 2. (a) *GW* quasiparticle spectral weight Z for $La_3Ni_2O_7$ at 29.5 GPa. The blue dots area on the *GW* bandplot (blue lines) indicates the QP weight Z with a specific scaling that ranges from minimum to maximum values (on the full BZ), indicated by the dots size in the legend. For reference, we show also the PBE band plot (gray lines). (b) *GW* band plot reporting the PWF orbital characters by the width of the lines with different colors. For more detailed projections, see Supplemental Material [66] Sec. VI.

pocket has an almost pure d_{z^2} character and is consistently present in PBE (or LDA) calculations.

The *GW* Fermi surface, in contrast, has no γ hole-pockets, as shown in Fig. 1(b). This result is totally consistent with experimental ARPES data [56], with respect to which we provide a detailed comparison in Sec. III B below, since it was performed at ambient pressure. This difference between DFT and *GW* is due to a slight downward shift ($70 \sim 80$ meV) of the lower Ni-$3d_{z^2}$ band along the XP direction [see Fig. 1(d)]. The absence of the γ pocket in experiment has been discussed also in the literature, and several semi-empirical corrections have been shown to reconcile theoretical calculations with the ARPES experiment. These methods either include the use of a weighted Fock exchange operator, as by HSE [54] or any other hybrid approach; or place more strength on correlation by introducing a Hubbard repulsion term of $U > 3.5$ eV on Ni-$3d_{z^2}$ electrons, like it was done in the calculation of Yang *et al.* [56], with the effect to lower this band. On the basis of this fact, Yang *et al.* [56] concluded that $La_3Ni_2O_7$ is a strongly correlated system. Here we show that, a calculation using physical quasiparticle energies out of a many-body self-energy, even in a non self-consistent *GW* approximation, is enough to get rid of the γ sheet at the Fermi level and achieve good agreement with the experiment. Our results are in line with the findings of Ryee *et al.* [55] who excluded both a transition to a Mott insulator or bad metal scenario.

The disappearance of the γ hole pocket has also been reported in a previous *GW* work [45] [see Fig. 1(c) for k-point correspondence]. They performed a G_0W_0 calculation based on a reduced four-orbital tight-binding model restricted to the Ni-e_g manifold. This model does not include the La-$5d_{x^2-y^2}$ band, which, as we will discuss in the next section, plays a nonnegligible role in the low energy spectrum. Their model also employs an effective screening that is renormalized to account for the missing degrees of freedom, and refers to the *Fmmm* structural phase.

Despite these significant methodological differences, our results are in remarkable agreement with theirs regarding the absence of the γ pocket. However, Christiansson *et al.* do not further comment on this disappearance in their G_0W_0 calculation, because their subsequent EDMFT simulations—performed on top of both DFT and G_0W_0—reintroduce and even enhance the spectral weight of the lower Ni-$3d_{z^2}$ band at the Fermi level. On this basis, they conclude that "the dominance of the d_{z^2} orbital distinguishes $La_3Ni_2O_7$ from the infinite-layer nickelates or the cuprates," which are instead dominated by $d_{x^2-y^2}$ character. This interpretation is not supported by our *GW* results (see Sec. III A 4 for the spectral weights), which show a predominantly $d_{x^2-y^2}$ character at low energy. Our findings rather align with the recent G_0W_0 calculations of You *et al.* [15].

Interestingly, Ryee *et al.* [55] found the γ pocket in both DFT and dynamical mean-field theory (DMFT) calculations, but not in cluster-DMFT (CDMFT) which is therefore more in agreement with the *GW* finding. This is an indication that nonlocal correlations, as provided by a CDMFT or a *GW* k-dependent self-energy, are important to describe such modification of the Fermi surface topology. However, CDMFT also find an important modification to the cuprate-shape β sheet which loses most of its 1D character (see below). On this point *GW* is more in agreement with DFT and local DMFT rather than with CDMFT.

2. La-$5d_{x^2-y^2}$ band lowering and self-doping

Beside this important qualitative modification of the Fermi surface, *GW* correlation corrections induce an even more evident and quantitative change in the bandwidth of the $5d_{x^2-y^2}$ band contributed by the two La spacer atoms only (i.e., with no contribution by the La inner atom lying in between the NiO planes, see Fig. S8 in Supplemental Material [66]). This La-$5d_{x^2-y^2}$ band, which in DFT-PBE is well above the Ni-$3d_{z^2}$

one, is lowered by *GW* corrections, as it can be seen at Γ in Fig. 1(d). At the *M* point, which is often overlooked in 2D calculations restricted to the $k_z = 0$ plane only, the lowering in *GW* is so large (∼0.7 eV) that the La-5$d_{x^2-y^2}$ crosses the Ni-3d_{z^2} band and becomes the lowest lying conduction band at M. Due to this large *GW* correction, the bottom of conduction (BOC) of the La-5$d_{x^2-y^2}$ band at M is situated just only 30 meV above the top of valence (TOV) of the Ni-3d_{z^2} band at P (in the following, we will refer to this TOV-BOC distance of 30 meV as the *indirect gap*). As a consequence, the *GW* Fermi level results from a delicate equilibrium between these two *incipient bands*: the Ni-3d_{z^2} band, which tends to open a γ pocket of holes at the BZ corners; and the La-5$d_{x^2-y^2}$ one, which tends to open a pocket of electrons at M, hereafter labeled λ. In the latter case, states located on the La atoms of the spacer start to be occupied instead of Ni e_g states. This results in an effective *self-doping* (SD) by holes of the NiO_2 planes. Note that a possible role of rare-earth self-doping was suggested [45] as responsible for the suppression of charge order, thereby possibly favoring superconductivity.

We can expect that any tiny perturbation of the system, e.g., doping, vacancies or defects, can drive the system to a qualitatively different electronic structure and Fermi surface, and therefore affect the superconductivity. Note that even computationally, these low-energy features are highly sensitive to the uncertainty of the integration method to calculate the Fermi level, which we discuss in further detail in Supplemental Material [66] Sec. IV. We mention two recent works which pointed out the shift of the La-5$d_{x^2-y^2}$ band due to correlations [15] and highlight the importance of this band on the screening which affects correlations on the Ni-e_g bands [71]. The latter work remarked in particular some coincidences between the lowering trend of the La-5$d_{x^2-y^2}$ band with pressure and the shape of the superconducting region. In our *GW* calculation this band reaches the Fermi level at lower pressures and crosses the Fermi level already at 30 GPa at the M point, in comparison to 80 Gpa at the Γ point in Verraes *et al.* [71].

3. Upper-lower Ni-3d_{z^2} energy gap

A feature of the electronic structure that is considered of particular interest in relation to the emergence of superconductivity in $La_3Ni_2O_7$ is the energy difference between the upper and lower Ni-3d_{z^2} bands. In the literature they are often labeled as bonding- and antibonding (as we explain in Supplemental Material [66] Sec. IX, we find that this labeling is not appropriate). This energy difference is related to the Ni interlayer hopping. According to the scenario proposed by Sakakibara *et al.* [24], a superconductivity gap would open on these two Ni-3d_{z^2} bands even though they can be as far as 1 eV away from the Fermi level, while the SC gap would be almost zero for the more Ni-3$d_{x^2-y^2}$ character bands crossing the Fermi level. In this scenario, a key parameter is precisely this Ni-3d_{z^2} interlayer hopping. As it can be seen in Fig. 1(d), the two Ni-3d_{z^2} are practically unaffected by *GW* corrections, as their band width and separation remain essentially the same as in the DFT calculation. On this point our calculation is in disagreement both with the *GW* calculation of Christiansson *et al.* [45], which found a negative downward shift of the upper band of ~ -0.25 eV at the BZ corner, and with the calculation of You *et al.* [15], which in contrast found a positive upward shift of ∼0.30 eV. Accordingly, our results leave practically unaffected the scenario proposed by Sakakibara *et al.* [24], while it would be boosted or disrupted in the two other cases.

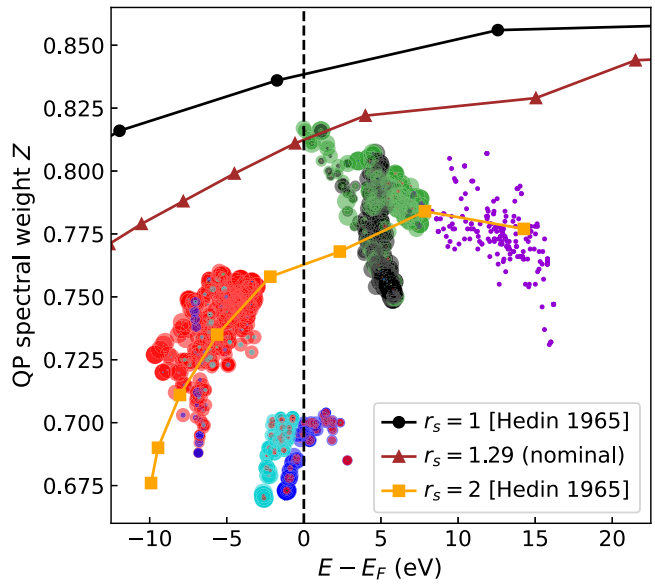

FIG. 3. QP spectral weights Z with respect to *GW* quasi particle energies with orbital characters corresponding to the ones of Fig. 2(b), except for the La-4f which are separated from the La-5d and plotted in black. Points for which the orbital character projection was not calculated are shown in purple. We observe an overall Fermi liquid behavior, though at a higher correlation level wrt the nominal density ($r_s = 2$ vs 1.29), and also its departure for the Ni-3d bands close to E_F.

4. GW quasiparticle spectral weight and 1D character

A *GW* calculation can also provide the quasiparticle spectral weight Z which represents a measure of the degree of correlation of the system. In Fig. 2(a) we show the interpolated *GW* bandplot of $La_3Ni_2O_7$ at 29.5 GPa, with the dots corresponding to the *GW* energies sampled on the 6 × 6 × 6 k-mesh. The relative size of the dots indicates the corresponding value of Z. In Fig. 2(b) we show the general orbital character of the *GW* bands (for more detailed projections, see Fig. S9 in Supplemental Material [66]). These plots are complemented with Fig. 3 which illustrates the behavior of Z as a function of the energy.

We note that La-5d bands, followed by the 4f, present the maximum QP weight culminating at $Z = 0.82$. This is already quite remarkable, in particular for the most localized f flat bands. Some of the La bands, in particular the previously discussed La-5$d_{x^2-y^2}$ which almost achieved the Fermi level, bring these high spectral weights lower in energy than the main La manifold located around 5 eV. For La-5d states above 5 eV, the QP weight is slightly decreasing. On the other side of the Fermi level, we also observe for the O-2p manifold below −3 eV a reduced Z with increasing distance from E_F with values ranging from 0.75 to 0.70. This is surprisingly lower than for La-5d and 4f states. However, the most remarkable

fact is that the Ni-3d bands, with no difference between e_g and t_{2g}, present the lowest weight of all quasiparticle states. For these states we observe a nonnegligible Z drop of up to 0.15 when compared in particular with the La-5$d_{x^2-y^2}$ which at M is situated at the same Fermi level as the Ni-3d. This fact points to a larger weight of the noncoherent part of the spectrum for the Ni-3d states.

For comparison, in Fig. 3 we also report the Z of the jellium model as in the Hedin GW calculation at $r_s = 1$ and 2 [59], as well as at the $La_3Ni_2O_7$ nominal average density of $r_s = 1.29$ at 29.5 GPa ($r_s = \sqrt[3]{3V/4\pi n_{\rm el}}$ with $V = 997$ a.u., the unit cell volume, and $n_{\rm el} = 111$ the number of correlated electrons entering into the self-energy from the chosen pseudopotentials). The GW general trend for a Fermi liquid is a reduction of the quasiparticle weight when going from the Fermi level to lower energies. Indeed, when going to the lowest energy quasiparticle states, the noncoherent part of spectra due to, e.g., plasmon losses, should increase, and correspondingly Z decreases. The same happens in the other higher energies direction, although not monotonically at the beginning (for $r_s = 1$ and 1.29, this decrease of Z occurs outside the plot range). From this, we can conclude that already with the correlations introduced by a non-self-consistent G_0W_0 approximation, $La_3Ni_2O_7$ show a Fermi liquid trend for all quasiparticle states. We can associate the O-2p and even the La-5d and La-4f quasiparticle weights to the $r_s = 2$ curve, that is to a higher level of correlation with respect to the system nominal density. On their side, the Ni-3d states show a departure from this Fermi liquid trend and so a even higher degree of correlation, although the minimal value of $Z = 0.67$ is still large enough not to configure a full breakdown of the Fermi liquid toward a strongly correlated picture. Of course, this is the picture emerging from a GW calculation which could be confuted by future experimental measures of the Z. Should a Fermi liquid breakdown be measured, we will have a failure of the GW approximation pointing to the need to go beyond it.

As shown in Figs. 1(a) and 1(b), the Fermi surface of $La_3Ni_2O_7$ exhibits negligible dispersion along the k_z direction, highlighting the pronounced 2D character of its electronic structure. We note that, while this situation is similar to what is found in most of the cuprates, it differs from the infinite-layer nickelates case that presents large k_z dispersion which introduces 3D features in their Fermi surface [72,73]. Moreover, we note that the dispersion of the Fermi surface of $La_3Ni_2O_7$ along k_x and k_y is also very weak. In fact, the α and β Fermi surface sheets can effectively be seen as a superposition of two sets of parallel planes along k_x and k_y, respectively. That is, as the superposition of 1D Fermi surfaces. These effectively 1D Fermi surfaces is an important difference with respect to cuprates. In particular, the emergence of $(\pi, 0)$ or $(0, \pi)$ spin-density-wave orders—as opposed to the (π, π) antiferromagnetic order characteristic of the cuprates—can be related to their nesting properties [34].

In the cuprates, ARPES experiments have revealed the emergence of so-called "Fermi arcs." Specifically, the quasiparticle spectral weight Z is found to be locally suppressed at points along the Fermi surface that would coincide with the 1D Fermi surface segments. Unfortunately, to check whether a similar phenomenon takes place in $La_3Ni_2O_7$, the $6 \times 6 \times 6$ k-sampling we have used in our GW calculation is not precise enough. Nevertheless, any experimental indication along this direction might provide a clue to understand superconductivity in both nickelates and cuprates.

B. Evolution with pressure

To gain further insight on the key aspects that might be relevant for superconductivity in $La_3Ni_2O_7$, we also analyze the evolution of its electronic structure with pressure. We remind that $La_3Ni_2O_7$ enters into a superconducting phase at an experimentally measured pressure of 14 GPa without doping [1].

To explore the largest range, we have included in our study a *fictitious* zero pressure phase of $La_3Ni_2O_7$ enforced in the tetragonal $I4/mmm$ crystal structure, which in reality at 0 GPa should be unstable toward the orthorhombic *Amam* phase with tilted octahedra. Of course, at the present knowledge we cannot exclude that the structural transition occurs at the same critical pressure as the transition to superconductivity, so that it is an important ingredient to explain the superconductivity in this system. In this case, our calculation of the tetragonal phase at 0 GPa would be probably inadequate to study the normal-superconducting phase transition. But beyond the fact that a GW calculation is less cumbersome in systems with more symmetries, our choice is motivated by the fact that the comparison of electronic structures is difficult between different crystal structures. Topological variations in the Fermi surface might trigger the superconducting phase transition (and maybe also the structural one): the approach proposed in this section focus on them.

In Fig. 4 we compare the GW electronic structure of $La_3Ni_2O_7$ at ambient pressure and at 29.5 GPa (in the same figure we also report the band plot of a biaxial strained $La_3Ni_2O_7$ which will be discussed in the next section). The most remarkable difference between the two pressures is in the La-5$d_{x^2-y^2}$ band at the point M which, at ambient pressure, lies $\sim$0.25 eV above the upper Ni-3d_{z^2} band in a very similar way to what already seen but at the DFT-PBE level in the 29.5 GPa case [see Fig. 1(d)], though in the latter the effect is much larger (0.5 eV). That is, correlations and pressure act in the same direction toward the emergence of the La-5$d_{x^2-y^2}$ band at the lowest energies. For a more complete discussion on this point, see Supplemental Material [66] Sec. II. At ambient pressure the La-5$d_{x^2-y^2}$ band is not present in the low energy region, and therefore the delicate balance between the two incipient self-doping bands is lost.

The electronic structure of $La_3Ni_2O_7$ at ambient pressure has been measured by an ARPES experiment [56] which we can now compare with our GW calculation at zero GPa. The γ hole pocket, which is found in the DFT PBE Fermi surface as due to the lower Ni-3d_{z^2} band, is absent in the ARPES experiment, exactly like in GW (Fig. 1(b) and Fig. S12 in the Supplemental Material [66]). ARPES spectra situate the top of this band at the BZ corners and 50 meV below the Fermi level. Our GW calculation at zero GPa (see Fig. 4), found the top of this band $\sim$50 meV below the Fermi level at the X k-point (corresponding to $\overline{\Gamma}'$ in Yang *et al.* [56], see Fig. 1(c) for k-points correspondence). In contrast to the La-5$d_{x^2-y^2}$ band, this lower Ni-3d_{z^2} band is almost unaffected by hydrostatic pressure: in the GW results at 29.5 GPa it just only shifts down

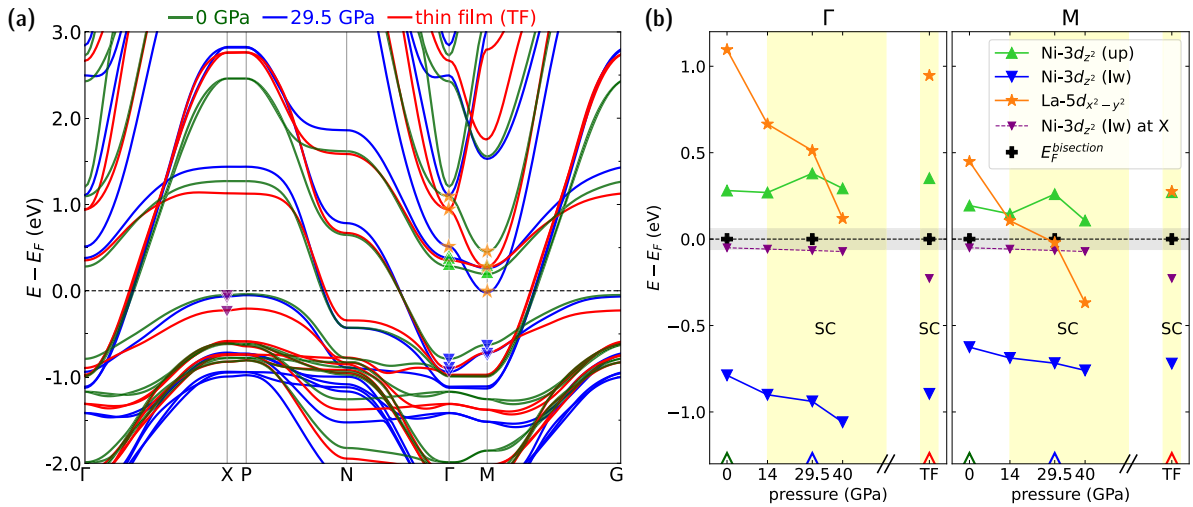

FIG. 4. (a) G_0W_0 Wannier interpolated band plot for $La_3Ni_2O_7$ at ambient pressure (green), at 29.5 GPa (blue) and under substrate strain which simulate a thin film (TF, red). (b) Evolution with pressure of selected features, identified with corresponding markers on panel (a). Upper and lower d_{z^2} bands are designated by up and lw, respectively. For the calculations at 14 and 40 GPa where the Fermi level was not calculated (because *GW* energies where not sampled on the full BZ), E_F has been estimated by a linear interpolation on the difference $E(3d_{z^2}^{\text{lower}}(\text{X})) - E_F^{\text{bisection}}$ (purple) from the calculations where E_F was available (black plus signs).

∼65 meV, which validates the comparison of the latter case with the ARPES, even if not performed at the same pressure.

In Fig. 4(b), we report a graph presenting the top-of-valence (TOV) and bottom-of-conduction (BOC) positions of the most relevant bands for different hydrostatic pressures. We report extra calculations done at 14 and at 40 GPa, covering the range of superconductivity as measured experimentally in Sun *et al.* [1]. The indirect gap is at its minimum around 29.5 GPa, and the La-5$d_{x^2-y^2}$ band is clearly self-doping beyond. From the same figure we can also remark that the same La-5$d_{x^2-y^2}$ band crosses the Ni-3d_{z^2} upper band precisely at 14 GPa, which is precisely the onset of the superconducting region measured by Sun *et al.* [1]. This might be just only a coincidence or have deeper implications. (Note that the position of this crossing and the overall picture does not change by performing a calculation in the ambient and low pressure *Amam* structure which will place the position of this band at even larger energy with respect to its *I*4/*mmm* position shown in Fig. 4 at 0 GPa, see Supplemental Material [66] Sec. III). In support to the latter, we cite a very recent work [71] which also found a correlation between the position of the La-5$d_{x^2-y^2}$ band with respect to the Fermi level, and the shape of the superconducting region. Their calculation is at the DFT level, so that they missed the earlier coincidence in pressure of the La-5$d_{x^2-y^2}$ with the Ni-3d_{z^2} band precisely at the onset of superconductivity at 14 GPa, but the relevance of the La-5$d_{x^2-y^2}$ for superconductivity has been remarked. We can more carefully conclude that both correlations and pressure are fundamental to describe the electronic structure of $La_3Ni_2O_7$ in its superconducting phase. In the next section we will see that *xy*-plane strain plays a similar role to correlations and pressure.

C. $La_3Ni_2O_7$ under epitaxial strain

Recent works [5,6] have reported superconductivity at $T_c > 40$ K in $La_3Ni_2O_7$ thin films under compressive strain at ambient pressure. Here we present the electronic structure of a bulk $La_3Ni_2O_7$ with a 1.8% strained $a = 3.77$ Å and a relaxed c, which we use to simulate the experimental thin film. The corresponding PBE and *GW* band plots, PDOS and DOS are shown in Fig. 5. In comparison to the previously discussed case at ambient and 29.5 GPa (see also Fig. 4), the electronic structure retains most of its features. The Fermi level crossing is practically the same in the three different cases. In particular, the β cuprate-like sheet has exactly the same shape (refer to Fig. 1). The lower Ni-3d_{z^2} band is significantly further from E_F in the thin film case (~ -0.2 eV). However, we observe two important differences. First, the γ hole pocket is already absent at the DFT level, that is the lower Ni-3d_{z^2} band does not cross E_F any longer, an effect that is further enhanced by *GW*. Second, the La-5$d_{x^2-y^2}$ band at M, which also undergoes a large negative *GW* correction of almost 1 eV, now stays above the Fermi level by ∼0.3 eV. In fact, it only reaches the upper Ni-3d_{z^2} band without crossing it. We can see that, with respect to the band positions at M, the epitaxial strained configuration is intermediate between 29.5 GPa and ambient pressure. Although our biaxial strain simulation implements a nonhydrostatic realization, we can compare it to the hydrostatic pressure case where the La-5$d_{x^2-y^2}$ BOC is degenerate with Ni-3d_{z^2} BOC at M. Following this analogy, from Fig. 4(b), where we have also reported the band positions for the thin film, we can tentatively attribute our epitaxial strain simulation as equivalent to the 14 GPa hydrostatic pressure case, that is precisely at the superconducting onset. This could be an indication that the relative position and overlap of BOC at M, might play a role as a triggering mechanism of superconductivity.

ARPES spectra have been measured on 1, 2, and 3 unit-cell epitaxial $La_{2.85}Pr_{0.15}Ni_2O_7$ films grown on $SrLaAlO_4$ substrates [57]. It is claimed that, in addition to the α and β sheets, the γ pocket is also present at the Fermi level. In another more recent ARPES experiment on a $La_2PrNi_2O_7$ thin film [74], the γ pocket is absent from the Fermi level and the

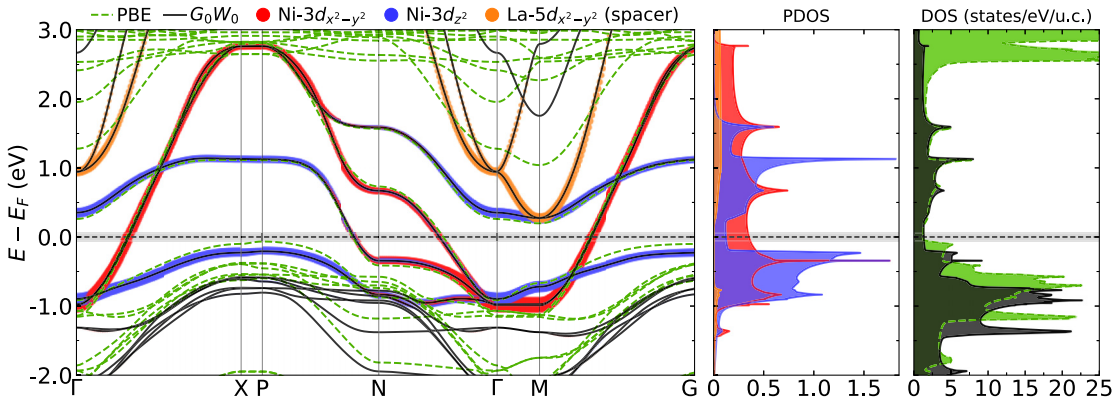

FIG. 5. PBE (dashed green) and G_0W_0 (black) band plots, DOS, and PDOS of $La_3Ni_2O_7$ thin film under substrate constraint. For the associated Fermi surfaces, see Fig. S11 in the Supplemental Material [66].

Ni-3d_{z^2} band is found 70 meV below the Fermi energy, which compares more favorably with our *GW* result of −200 meV. In any case, the comparison with our *GW* electronic structure is difficult because they considered a Pr doped system. From our side, we did not include the neighborhood effect of the substrate which is certainly affecting the electronic structure of such thin films. Our results should then be considered as an *ab initio* prediction of the electronic structure which could be measured for a $La_3Ni_2O_7$ thin film of enough large thickness. Or, possibly, for a nonhydrostatic planar strain applied on a bulk sample that can be realized experimentally by applying a tensile strain to the *c* axis, which will induce a biaxial compressive strain of the *ab* plane by Poisson law.

We can conclude that our *GW* calculation on the epitaxial strained case presents an electronic structure very similar to the bulk at 14 GPa pressure. Correlation effects are very important on both the lower Ni-3d_{z^2} band, causing the disappearance of the γ pocket, and on the increased relevance of the La-5$d_{x^2-y^2}$ band at low energy [75,76].

IV. CONCLUSIONS

In conclusion, we have studied pressure and biaxial strain effects on the electronic structure of $La_3Ni_2O_7$, taking into account correlation effects within the *ab initio GW* approximation to the self-energy. We confirm that the electronic structure of $La_3Ni_2O_7$ is extremely sensitive to the internal atomic positions of its crystal structure. *GW* correlation effects shift downward the lower Ni-3d_{z^2} band, so to remove the γ hole pocket from the Fermi level without introducing any adjustable parameter. Therefore, the *GW* Fermi surface is composed only of the cuprate-shape sheet β plus the nickelate-specific cylinder α, both showing an effective 1D character, and is in good agreement with ARPES experiments [56] which did not find any γ pocket. Additionally, we observe a nonnegligible drop in the *GW* quasiparticle spectral weight on the Ni-3*d* states, both e_g and t_{2g}, so to configure a little departure from a Fermi liquid behavior. Finally, we have shown that not only correlations, but also pressure or biaxial strain play a crucial role in pulling down the La-5$d_{x^2-y^2}$ band at Γ and M toward the Fermi level, which may induce self-doping. In any case, at pressures and strains of interest of superconductivity, this band might play an important role at low energy, a fact which is often overlooked in effective-model studies.

ACKNOWLEDGMENTS

We thank Markus Holzmann for useful discussions. We acknowledge financing from the LABEX LANEF Project NICOS. Computing time has been provided by French GENCI Grant No. 2022-AD01091394 and Grenoble CIGRID.

DATA AVAILABILITY

The data that support the findings of this article are not publicly available. The data are available from the authors upon reasonable request.

[1] H. Sun, M. Huo, X. Hu, J. Li, Z. Liu, Y. Han, L. Tang, Z. Mao, P. Yang, B. Wang, J. Cheng, D.-X. Yao, G.-M. Zhang, and M. Wang, Signatures of superconductivity near 80 K in a nickelate under high pressure, Nature (London) **621**, 493 (2023).

[2] N. Wang, G. Wang, X. Shen, J. Hou, J. Luo, X. Ma, H. Yang, L. Shi, J. Dou, J. Feng, J. Yang, Y. Shi, Z. Ren, H. Ma, P. Yang, Z. Liu, Y. Liu, H. Zhang, X. Dong, Y. Wang *et al.*, Bulk high-temperature superconductivity in pressurized tetragonal $La_2PrNi_2O_7$, Nature (London) **634**, 579 (2024).

[3] Q. Li, Y.-J. Zhang, Z.-N. Xiang, Y. Zhang, X. Zhu, and H.-H. Wen, Signature of superconductivity in pressurized $La_4Ni_3O_{10}$, Chin. Phys. Lett. **41**, 017401 (2024).

[4] J. Li, D. Peng, P. Ma, H. Zhang, Z. Xing, X. Huang, C. Huang, M. Huo, D. Hu, Z. Dong, X. Chen, T. Xie, H. Dong, H. Sun, Q. Zeng, H.-k. Mao, and M. Wang, Identification of the superconductivity in bilayer nickelate $La_3Ni_2O_7$ under high pressure up to 100 GPa, Natl. Sci. Rev. nwaf220 (2025).

[5] E. K. Ko, Y. Yu, Y. Liu, L. Bhatt, J. Li, V. Thampy, C.-T. Kuo, B. Y. Wang, Y. Lee, K. Lee, J.-S. Lee, B. H. Goodge,

D. A. Muller, and H. Y. Hwang, Signatures of ambient pressure superconductivity in thin film $La_3Ni_2O_7$, Nature (London) **638**, 935 (2025).

[6] G. Zhou, W. Lv, H. Wang, Z. Nie, Y. Chen, Y. Li, H. Huang, W.-Q. Chen, Y.-J. Sun, Q.-K. Xue, and Z. Chen, Ambient-pressure superconductivity onset above 40 K in $(La, Pr)_3Ni_2O_7$ films, Nature **640**, 641 (2025).

[7] Z. Li and S. G. Louie, Two-gap superconductivity and the decisive role of rare-earth *d* electrons in infinite-layer nickelates, Phys. Rev. Lett. **133**, 126401 (2024).

[8] Q. N. Meier, J. B. de Vaulx, F. Bernardini, A. S. Botana, X. Blase, V. Olevano, and A. Cano, Preempted phonon-mediated superconductivity in the infinite-layer nickelates, Phys. Rev. B **109**, 184505 (2024).

[9] Y. Nomura, M. Hirayama, T. Tadano, Y. Yoshimoto, K. Nakamura, and R. Arita, Formation of a two-dimensional single-component correlated electron system and band engineering in the nickelate superconductor $NdNiO_2$, Phys. Rev. B **100**, 205138 (2019).

[10] S. Di Cataldo, P. Worm, L. Si, and K. Held, Absence of electron-phonon-mediated superconductivity in hydrogen-intercalated nickelates, arXiv:2304.03599.

[11] S. Di Cataldo, P. Worm, J. M. Tomczak, L. Si, and K. Held, Unconventional superconductivity without doping in infinite-layer nickelates under pressure, Nat. Commun. **15**, 3952 (2024).

[12] Y. Lee, X. Wei, Y. Yu, L. Bhatt, K. Lee, B. H. Goodge, S. P. Harvey, B. Y. Wang, D. A. Muller, L. F. Kourkoutis, W.-S. Lee, S. Raghu, and H. Y. Hwang, Synthesis of superconducting freestanding infinite-layer nickelate heterostructures on the millimetre scale, Nat. Synth. **4**, 573 (2025).

[13] S. L. E. Chow, Z. Luo, and A. Ariando, High-temperature superconducting oxide without copper at ambient pressure, arXiv:2410.00144.

[14] Z. Ouyang, M. Gao, and Z.-Y. Lu, Absence of electron-phonon coupling superconductivity in the bilayer phase of $La_3Ni_2O_7$ under pressure, npj Quantum Mater. **9**, 80 (2024).

[15] J.-Y. You, Z. Zhu, M. Del Ben, W. Chen, and Z. Li, Unlikelihood of a phonon mechanism for the high-temperature superconductivity in $La_3Ni_2O_7$, npj Comput. Mater. **11**, 3 (2025).

[16] M. Nakata, D. Ogura, H. Usui, and K. Kuroki, Finite-energy spin fluctuations as a pairing glue in systems with coexisting electron and hole bands, Phys. Rev. B **95**, 214509 (2017).

[17] Y. Zhang, L.-F. Lin, A. Moreo, and E. Dagotto, Electronic structure, dimer physics, orbital-selective behavior, and magnetic tendencies in the bilayer nickelate superconductor $La_3Ni_2O_7$ under pressure, Phys. Rev. B **108**, L180510 (2023).

[18] Z. Luo, X. Hu, M. Wang, W. Wú, and D.-X. Yao, Bilayer two-orbital model of $La_3Ni_2O_7$ under pressure, Phys. Rev. Lett. **131**, 126001 (2023).

[19] Y. Gu, C. Le, Z. Yang, X. Wu, and J. Hu, Effective model and pairing tendency in bilayer Ni-based superconductor $La_3Ni_2O_7$, Phys. Rev. B **111**, 174506 (2025).

[20] Z. Luo, B. Lv, M. Wang, W. Wú, and D.-X. Yao, High-T_c superconductivity in $La_3Ni_2O_7$ based on the bilayer two-orbital *t*-*J* model, npj Quantum Mater. **9**, 61 (2024).

[21] Q.-G. Yang, D. Wang, and Q.-H. Wang, Possible $s_\pm$-wave superconductivity in $La_3Ni_2O_7$, Phys. Rev. B **108**, L140505 (2023).

[22] F. Lechermann, J. Gondolf, S. Bötzel, and I. M. Eremin, Electronic correlations and superconducting instability in $La_3Ni_2O_7$ under high pressure, Phys. Rev. B **108**, L201121 (2023).

[23] Y. Shen, M. Qin, and G.-M. Zhang, Effective bi-layer model Hamiltonian and density-matrix renormalization group study for the high-T_c superconductivity in $La_3Ni_2O_7$ under high pressure, Chin. Phys. Lett. **40**, 127401 (2023).

[24] H. Sakakibara, N. Kitamine, M. Ochi, and K. Kuroki, Possible high T_c superconductivity in $La_3Ni_2O_7$ under high pressure through manifestation of a nearly half-filled bilayer Hubbard model, Phys. Rev. Lett. **132**, 106002 (2024).

[25] C. Lu, Z. Pan, F. Yang, and C. Wu, Interlayer coupling driven high-temperature superconductivity in $La_3Ni_2O_7$ under pressure, Phys. Rev. Lett. **132**, 146002 (2024).

[26] Z. Liao, L. Chen, G. Duan, Y. Wang, C. Liu, R. Yu, and Q. Si, Electron correlations and superconductivity in $La_3Ni_2O_7$ under pressure tuning, Phys. Rev. B **108**, 214522 (2023).

[27] X.-Z. Qu, D.-W. Qu, J. Chen, C. Wu, F. Yang, W. Li, and G. Su, Bilayer *t*-*J*-$J_\perp$ model and magnetically mediated pairing in the pressurized nickelate $La_3Ni_2O_7$, Phys. Rev. Lett. **132**, 036502 (2024).

[28] Y.-F. Yang, G.-M. Zhang, and F.-C. Zhang, Interlayer valence bonds and two-component theory for high-T_c superconductivity of $La_3Ni_2O_7$ under pressure, Phys. Rev. B **108**, L201108 (2023).

[29] W. Wú, Z. Luo, D.-X. Yao, and M. Wang, Superexchange and charge transfer in the nickelate superconductor $La_3Ni_2O_7$ under pressure, Sci. China Phys. Mech. Astron. **67**, 117402 (2024).

[30] J. Huang, Z. D. Wang, and T. Zhou, Impurity and vortex states in the bilayer high-temperature superconductor $La_3Ni_2O_7$, Phys. Rev. B **108**, 174501 (2023).

[31] K. Jiang, Z. Wang, and F.-C. Zhang, High-temperature superconductivity in $La_3Ni_2O_7$, Chin. Phys. Lett. **41**, 017402 (2024).

[32] D.-C. Lu, M. Li, Z.-Y. Zeng, W. Hou, J. Wang, F. Yang, and Y.-Z. You, Superconductivity from doping symmetric mass generation insulators: Application to $La_3Ni_2O_7$ under pressure, arXiv:2308.11195.

[33] H. Oh and Y.-H. Zhang, Type II *t*-*J* model and shared antiferromagnetic spin coupling from Hund's rule in superconducting $La_3Ni_2O_7$, Phys. Rev. B **108**, 174511 (2023).

[34] Y. Zhang, L.-F. Lin, A. Moreo, T. A. Maier, and E. Dagotto, Structural phase transition, $s_\pm$-wave pairing, and magnetic stripe order in bilayered superconductor $La_3Ni_2O_7$ under pressure, Nat. Commun. **15**, 2470 (2024).

[35] T. Kaneko, H. Sakakibara, M. Ochi, and K. Kuroki, Pair correlations in the two-orbital Hubbard ladder: Implications for superconductivity in the bilayer nickelate $La_3Ni_2O_7$, Phys. Rev. B **109**, 045154 (2024).

[36] H. Yang, H. Oh, and Y.-H. Zhang, Strong pairing and symmetric pseudogap metal in double Kondo lattice model: from nickelate superconductor to tetralayer optical lattice, arXiv:2408.01493.

[37] H. Yang, H. Oh, and Y.-H. Zhang, Strong pairing from a small Fermi surface beyond weak coupling: Application to $La_3Ni_2O_7$, Phys. Rev. B **110**, 104517 (2024).

[38] D. A. Shilenko and I. V. Leonov, Correlated electronic structure, orbital-selective behavior, and magnetic correlations in double-layer $La_3Ni_2O_7$ under pressure, Phys. Rev. B **108**, 125105 (2023).

[39] Y.-H. Tian, Y. Chen, J.-M. Wang, R.-Q. He, and Z.-Y. Lu, Correlation effects and concomitant two-orbital $s_{\pm}$-wave superconductivity in $La_3Ni_2O_7$ under high pressure, Phys. Rev. B **109**, 165154 (2024).

[40] Y.-B. Liu, J.-W. Mei, F. Ye, W.-Q. Chen, and F. Yang, $s_{\pm}$-wave pairing and the destructive role of apical-oxygen deficiencies in $La_3Ni_2O_7$ under pressure, Phys. Rev. Lett. **131**, 236002 (2023).

[41] Y. Cao and Y.-F. Yang, Flat bands promoted by Hund's rule coupling in the candidate double-layer high-temperature superconductor $La_3Ni_2O_7$, Phys. Rev. B **109**, L081105 (2024).

[42] Q. Qin and Y.-F. Yang, High-T_c superconductivity by mobilizing local spin singlets and possible route to higher T_c in pressurized $La_3Ni_2O_7$, Phys. Rev. B **108**, L140504 (2023).

[43] X. Chen, P. Jiang, J. Li, Z. Zhong, and Y. Lu, Charge and spin instabilities in superconducting $La_3Ni_2O_7$, Phys. Rev. B **111**, 014515 (2025).

[44] R. Jiang, J. Hou, Z. Fan, Z.-J. Lang, and W. Ku, Pressure driven fractionalization of ionic spins results in cupratelike high-T_c superconductivity in $La_3Ni_2O_7$, Phys. Rev. Lett. **132**, 126503 (2024).

[45] V. Christiansson, F. Petocchi, and P. Werner, Correlated electronic structure of $La_3Ni_2O_7$ under pressure, Phys. Rev. Lett. **131**, 206501 (2023).

[46] Y. Zhang, L.-F. Lin, A. Moreo, T. A. Maier, and E. Dagotto, Trends in electronic structures and $s_{\pm}$-wave pairing for the rare-earth series in bilayer nickelate superconductor $R_3Ni_2O_7$, Phys. Rev. B **108**, 165141 (2023).

[47] X.-W. Yi, Y. Meng, J.-W. Li, Z.-W. Liao, W. Li, J.-Y. You, B. Gu, and G. Su, Antiferromagnetic ground state, charge density waves and oxygen vacancies induced metal-insulator transition in pressurized $La_3Ni_2O_7$, Phys. Rev. B **110**, L140508 (2024).

[48] J. Chen, F. Yang, and W. Li, Orbital-selective superconductivity in the pressurized bilayer nickelate $La_3Ni_2O_7$: An infinite projected entangled-pair state study, Phys. Rev. B **110**, L041111 (2024).

[49] Y. Nomura, M. Kitatani, S. Sakai, and R. Arita, Strong-coupling high-T_c superconductivity in doped correlated band insulator, Phys. Rev. B **112**, L020504 (2025).

[50] D. K. Singh, G. Goyal, and Y. Bang, Possible pairing states in the superconducting bilayer nickelate, arXiv:2409.09321.

[51] H.-X. Xu, Y. Xie, D. Guterding, and Z. Wang, Competition of superconducting pairing symmetries in $La_3Ni_2O_7$ (2025), https://arxiv.org/html/2501.05254v1.

[52] C. Xia, H. Liu, S. Zhou, and H. Chen, Sensitive dependence of pairing symmetry on Ni-e_g crystal field splitting in the nickelate superconductor $La_3Ni_2O_7$, Nat. Commun. **16**, 1054 (2025).

[53] F. Lechermann, S. Bötzel, and I. M. Eremin, Electronic instability, layer selectivity, and Fermi arcs in $La_3Ni_2O_7$, Phys. Rev. Mat. **8**, 074802 (2024).

[54] Y. Wang, K. Jiang, Z. Wang, F.-C. Zhang, and J. Hu, Electronic and magnetic structures of bilayer $La_3Ni_2O_7$ at ambient pressure, Phys. Rev. B **110**, 205122 (2024).

[55] S. Ryee, N. Witt, and T. O. Wehling, Quenched pair breaking by interlayer correlations as a key to superconductivity in $La_3Ni_2O_7$, Phys. Rev. Lett. **133**, 096002 (2024).

[56] J. Yang, H. Sun, X. Hu, Y. Xie, T. Miao, H. Luo, H. Chen, B. Liang, W. Zhu, G. Qu, C.-Q. Chen, M. Huo, Y. Huang, S. Zhang, F. Zhang, F. Yang, Z. Wang, Q. Peng, H. Mao, G. Liu *et al.*, Orbital-dependent electron correlation in double-layer nickelate $La_3Ni_2O_7$, Nat. Commun. **15**, 4373 (2024).

[57] P. Li, G. Zhou, W. Lv, Y. Li, C. Yue, H. Huang, L. Xu, J. Shen, Y. Miao, W. Song, Z. Nie, Y. Chen, H. Wang, W. Chen, Y. Huang, Z.-H. Chen, T. Qian, J. Lin, J. He, Y.-J. Sun *et al.*, Angle-resolved photoemission spectroscopy of superconducting $(La, Pr)_3Ni_2O_7/SrLaAlO_4$ heterostructures, Natl. Sci. Rev. nwaf205 (2025), arXiv:2501.09255v1.

[58] Y. Gao, Robust $s_{\pm}$-wave pairing in a bilayer two-orbital model of pressurized $La_3Ni_2O_7$ without the γ Fermi surface, arXiv:2502.19840.

[59] L. Hedin, New method for calculating the one-particle Green's function with application to the electron-gas problem, Phys. Rev. **139**, A796 (1965).

[60] G. Strinati, H. J. Mattausch, and W. Hanke, Dynamical correlation effects on the quasiparticle Bloch states of a covalent crystal, Phys. Rev. Lett. **45**, 290 (1980).

[61] M. S. Hybertsen and S. G. Louie, First-principles theory of quasiparticles: Calculation of band gaps in semiconductors and insulators, Phys. Rev. Lett. **55**, 1418 (1985).

[62] R. W. Godby, M. Schlüter, and L. J. Sham, Quasiparticle energies in GaAs and AlAs, Phys. Rev. B **35**, 4170(R) (1987).

[63] J. P. Perdew, K. Burke, and M. Ernzerhof, Generalized gradient approximation made simple, Phys. Rev. Lett. **77**, 3865 (1996).

[64] X. Gonze, G.-M. Rignanese, M. Verstraete, J.-M. Beuken, Y. Pouillon, R. Caracas, F. Jollet, M. Torrent, G. Zerah, M. Mikami, P. Ghosez, M. Veithen, J.-Y. Raty, V. Olevano, F. Bruneval, L. Reining, R. Godby, G. Onida, D. R. Hamann, and D. C. Allan, A brief introduction to the ABINIT software package, Z. Kristall. **220**, 558 (2005).

[65] M. J. van Setten, M. Giantomassi, E. Bousquet, M. J. Verstraete, D. R. Hamann, X. Gonze, and G.-M. Rignanese, The PSEUDODOJO: Training and grading a 85 element optimized norm-conserving pseudopotential table, Comput. Phys. Commun. **226**, 39 (2018).

[66] See Supplemental Material at http://link.aps.org/supplemental/10.1103/q5ym-hf5k for details.

[67] R. W. Godby and R. J. Needs, Metal-insulator transition in Kohn-Sham theory and quasiparticle theory, Phys. Rev. Lett. **62**, 1169 (1989).

[68] P. Toulemonde *et al.* (unpublished).

[69] Y. Hinuma, G. Pizzi, Y. Kumagai, F. Oba, and I. Tanaka, Band structure diagram paths based on crystallography, Comput. Mater. Sci. **128**, 140 (2017).

[70] V. Olevano, F. Bernardini, X. Blase, and A. Cano, *Ab initio* many-body *GW* correlations in the electronic structure of $LaNiO_2$, Phys. Rev. B **101**, 161102(R) (2020).

[71] D. Verraes, T. Braeckevelt, N. Bultinck, and V. V. Speybroeck, Evidence for strongly correlated superconductivity in $La_3Ni_2O_7$ from first principles, arXiv:2502.19501v1.

[72] K.-W. Lee and W. E. Pickett, Infinite-layer $LaNiO_2$: Ni^{1+} is not Cu^{2+}, Phys. Rev. B **70**, 165109(R) (2004).

[73] F. Bernardini, V. Olevano, and A. Cano, Magnetic penetration depth and T_c in superconducting nickelates, Phys. Rev. Res. **2**, 013219 (2020).

[74] B. Y. Wang, Y. Zhong, S. Abadi, Y. Liu, Y. Yu, X. Zhang, Y.-M. Wu, R. Wang, J. Li, Y. Tarn, E. K. Ko, V. Thampy, M. Hashimoto, D. Lu, Y. S. Lee, T. P. Devereaux, C. Jia, H. Y. Hwang, and Z.-X. Shen, Electronic structure of compressively strained thin film $La_2PrNi_2O_7$, arXiv:2504.16372.

[75] I. Souza, N. Marzari, and D. Vanderbilt, Maximally localized Wannier functions for entangled energy bands, Phys. Rev. B **65**, 035109 (2001).

[76] P.-O. Löwdin, On the non-orthogonality problem connected with the use of atomic wave functions in the theory of molecules and crystals, J. Chem. Phys. **18**, 365 (1950).